Supporting Information for

Dual Function Organic Active Materials for Nonaqueous Redox Flow Batteries

N. Harsha Attanayake,[a,b] Zhiming Liang,[a] Yilin Wang,[c,d] Aman Preet Kaur, [a,b] Sean R. Parkin,[a] Justin K. Mobley,[a] Randy H. Ewoldt,[c,d] James Landon,[e,f] Susan A. Odom*,[a,b]

[a] *Department of Chemistry, University of Kentucky, Lexington, KY 40506, USA*
[b] *Joint Center for Energy Storage Research, University of Kentucky, Lexington, KY 40506, USA*
[c] *Department of Mechanical Science and Engineering, University of Illinois at Urbana-Champaign, Illinois 61820 USA*
[d] *Joint Center for Energy Storage Research, University of Illinois at Urbana-Champaign, Illinois 61820 USA*
[e] *Department of Chemical Engineering, University of Kentucky, Lexington, KY 40506, USA*
[f] *Center for Applied Energy Research, University of Kentucky, Lexington, KY 40511, USA*

I. Materials

Promethazine hydrochloride (98%) was purchased from Tokyo Chemical Incorporated. Bromoethane (≥ 99%), 4,4'-bipyridyl (anhydrous, 98%, stored in an argon filled glovebox), 1-bromo-2-(2-methoxyethoxy)ethane (≥ 90%), and lithium bis(trifluoromethylsulfonyl)imide (≥ 99%, stored in an argon filled glovebox) were purchased from Acros Organics. Acetonitrile (ACN, ≥ 99.9%) was purchased from J.T. Barker. *N,N* dimethylformamide (DMF, ≥ 99.9%), diethyl ether (anhydrous, ≥ 99%), and acetone (≥ 99%), were purchased from VWR. ACN and DMF were stored in a solvent purification system (L.T. Technologies). Tetraethylammonium bis(trifluoromethane) sulfonamide (TEATFSI, > 99%, stored in an argon filled glovebox) was purchased from IoLiTec. Conductivity standards were purchased from Oakton (1.413, 12.9, and 80 mS cm^{-1}) and RICCA (25 and 47.6 mS cm^{-1}). FAPQ 375 PP anion exchange membrane (75 μm) was purchased from FumaTech. ^{1}H, ^{19}F, and ^{13}C NMR spectra were obtained on 400 MHz Bruker Avance NEO (equipped with a Smart Probe) in DMSO-d_6 from Cambridge Isotope Laboratories. For ^{19}F NMR, chemical shifts are reported vs. $CFCl_3$ at 0 ppm by adjusting the chemical shift of internal reference hexafluorobenzene to -164.9 ppm. ESI mass spectra were obtained on a Thermo Finnigan LTQ ion trap mass spectrometer. Mass spectra were recorded in positive-ion mode. Elemental analysis was performed by Atlantic Microlab, Inc. Solubility tests, cyclic voltammetry measurements, and flow cell tests were performed in an argon-filled glovebox (MBraun, O_2 < 5 ppm, H_2O < 0.1 ppm).

II. Synthesis

Promethazine (PRT) was extracted from promethazine hydrochloride as previously reported.[1]

Ethylpromethazine bromide (EPRT-Br). To an oven-dried 500 mL round-bottomed flask containing a stir bar cooled under nitrogen atmosphere, promethazine (28.00 g, 0.0984 mol) was dissolved in anhydrous ACN (250 mL), creating a colorless solution. Then, bromoethane (11.1 mL 0.148 mol) was added to the reaction mixture and stirred for 24 h at room temperature during

which a white solid was formed. The reaction flask was immersed in an ice bath to completely precipitate the product. Then, product was filtered and washed with diethyl ether to remove unreacted starting materials. Finally, the product, a white solid, was dried in a vacuum oven at 50 °C and -100 kPa (24.6 g, 64%). ^{1}H NMR (400 MHz, DMSO-d_6) δ 7.39 – 7.14 (m, 6H), 7.04 (td, J = 7.4, 1.4 Hz, 2H), 4.64 (dd, J = 14.6, 4.2 Hz, 1H), 4.08 (dd, J = 14.5, 8.6 Hz, 1H), 3.71 (ddt, J = 13.2, 10.8, 6.4 Hz, 1H), 3.59 – 3.37 (m, 2H), 3.04 (d, J = 7.6 Hz, 6H), 1.37 (d, J = 6.5 Hz, 3H), 1.21 (t, J = 7.1 Hz, 3H). ^{13}C NMR (100 MHz, DMSO-d_6) δ 143.7, 127.3, 127.1, 124.8, 122.9, 116.1, 64.5, 57.1, 46.9, 46.5, 45.3, 11.6, 7.3. ESI-MS: *m/z* 313 (100%), 314 (22%), 315 (4%). Anal. Calcd. for $C_{19}H_{25}BrN_2S$ C, 58.01; H, 6.41; N, 7.12; Br, 20.31. Found C, 58.13; H, 6.37; N, 7.12; Br, 20.29.

Ethylpromethazine bis(trifluoromethanesulfonyl)imide (EPRT-TFSI). In an oven-dried 1 L round-bottomed flask containing a stir bar cooled under nitrogen atmosphere, EPRT-Br (15.00 g, 0.0381 mol) was dissolved in deionized (DI) water (300 mL), creating a colorless solution. Then, in an Erlenmeyer flask, LiTFSI (13.2 g, 0.046 mol) was dissolved in DI water (100 mL), and this solution was slowly added to the round-bottomed flask over a period of about 10 min, resulting in a milky solution. The reaction mixture was stirred for 3 h, at room temperature and the product precipitated upon completion of the reaction. The precipitated white solid was filtered and washed with DI water to remove unreacted starting materials. Finally, the isolated solid product (21.5 g, 95%) was dried in a vacuum oven at 50 °C and -100 kPa. To grow crystals of this product, a saturated solution of EPRT-TFSI in DCM was prepared in a glass vial fitted with a rubber septum. Then, the solvent was allowed to evaporate slowly under nitrogen after inserting a vent needle, and crystals formed at the bottom of glass vial. ^{1}H NMR (400 MHz, DMSO-d_6) δ 7.41 – 7.13 (m, 6H), 7.04 (t, J = 7.4 Hz, 2H), 4.63 (dd, J = 14.6, 4.2 Hz, 1H), 4.09 (dd, J = 14.6, 8.5 Hz, 1H), 3.85 – 3.60 (m, 1H), 3.60 – 3.37 (m, 2H), 3.04 (d, J = 6.9 Hz, 6H), 1.38 (d, J = 6.4 Hz, 3H), 1.21 (t, J = 7.1 Hz, 3H). ^{13}C NMR (100 MHz, DMSO-d_6) δ 143.2, 126.8, 126.5, 124.3, 122.4, 118.3 (q, J = 321.9 Hz), 115.6, 64.1, 56.6, 46.4, 45.9, 44.7, 11.1, 6.7. ^{19}F NMR (400 MHz, DMSO-d_6) δ -75.6 (vs. hexafluorobenzene). ESI-MS: *m/z* 313 (100%), 314 (22%), 315 (4%). Anal. Calcd. for $C_{21}H_{25}F_6N_3O_4S_3$ C, 42.29; H, 4.25; N, 7.08; F, 19.2. Found C, 42.54; H, 4.14; N, 7.07; F, 19.04.

Bis((2-(2 methoxyethoxy)ethyl))viologen bromide (MEEV-Br$_2$). To an oven-dried 1 L round-bottomed flask containing a stir bar cooled under a nitrogen atmosphere, 4,4-bipyridyl (20.00 g, 0.1284 mol) and anhydrous DMF (600 mL) were added, creating a yellow/orange solution. Then 1-bromo-2-(2-methoxyethoxy)ethane (51.7 mL 0.384 mol) was added at room temperature after which the reaction flask was immersed in an oil bath set at 100 °C and stirred for 24 h during which time a yellow precipitate formed. The reaction flask was removed from the oil bath and the reaction mixture was allowed to cool to room temperature. Then the resulting yellow solid was filtered under a blanket of nitrogen and was washed with isopropanol, acetone, and diethyl ether to remove unreacted starting materials. Finally, the product, a yellow solid, was dried in a vacuum oven at 50 °C and -100 kPa (41.5 g, 62%). ^{1}H NMR (400 MHz, DMSO-d_6) δ 9.31 (d, J = 6.4 Hz, 4H), 8.79 (d, J = 6.4 Hz, 4H), 4.88 (t, J = 4.8 Hz, 4H), 3.98 (t, J = 4.8 Hz, 4H), 3.58 (t, J = 4.2 Hz,

4H), 3.38 (t, J = 4.2 Hz, 4H), 3.17 (s, 6H). ^{13}C NMR (100 MHz, DMSO-d_6) δ 148.2, 145.6, 125.7, 70.4, 68.8, 68.0, 59.8, 57.5. ESI-MS: *m/z* 362 (100%), 363 (22%), 360 (14%). Anal. Calcd. for $C_{20}H_{30}Br_2N_2O_4$ C, 45.99; H, 5.79; N, 5.36; Br, 30.60. Found C, 44.87; H, 5.52; N, 5.48; Br, 30.86.

Bis((2-(2-methoxyethoxy)ethyl))viologen bis(trifluoromethanesulfonyl)imide (MEEV-(TFSI)$_2$). In a 1 L round-bottomed flask, MEEV-Br_2 (40.00 g, 0.07664 mol) was dissolved in DI water (600 mL), creating a pale orange solution. In another 250 mL round-bottomed flask, LiTFSI (49.5 g, 0.172 mol) was dissolved in DI water (100 mL), and the resultant solution was added to the flask containing MEEV-Br_2 over a period of about 10 min, resulting in a pale pink solution. The reaction mixture was stirred at room temperature for 3 h during which a precipitate formed. The pale pink precipitate was filtered and washed with water to remove unreacted starting materials. Finally, the solid product was dried in a vacuum oven at 50 °C and -100 kPa, yielding a pale pink solid (42.5 g, 60%). To obtain crystals of this product, the isolated solid was crystalized from water in the presence of charcoal yielding the product as white crystalline needles. ^{1}H NMR (400 MHz, DMSO-d_6) δ 9.30 (d, J = 6.6 Hz, 4H), 8.78 (d, J = 6.6 Hz, 4H), 4.88 (t, J = 5.0 Hz, 4H), 3.97 (t, J = 5.0 Hz, 4H), 3.57 (t, J = 4.4 Hz, 4H), 3.38 (t, J = 4.4 Hz, 4H), 3.17 (s, 6H). ^{13}C NMR (100 MHz, DMSO-d_6) δ 148.5, 145.7, 125.8, 119.6 (q, J = 321.9 Hz), 70.5, 69.1, 68.1, 60.1, 57.5. ^{19}F NMR (400 MHz, DMSO-d_6) δ -78.8 (vs. hexafluorobenzene). ESI-MS: *m/z* 362 (100%), 363 (23%), 360 (13%). Anal. Calcd. for $C_{24}H_{30}F_{12}N_2O_{12}S_4$ C, 31.24; H, 3.28; N, 6.07; F, 24.71. Found C, 30.94; H, 3.07; N, 6.05; F, 24.42.

III. Nuclear Magnetic Resonance Spectroscopy

^{1}H and ^{13}C NMR spectra of the compounds prepared here are shown in this section.

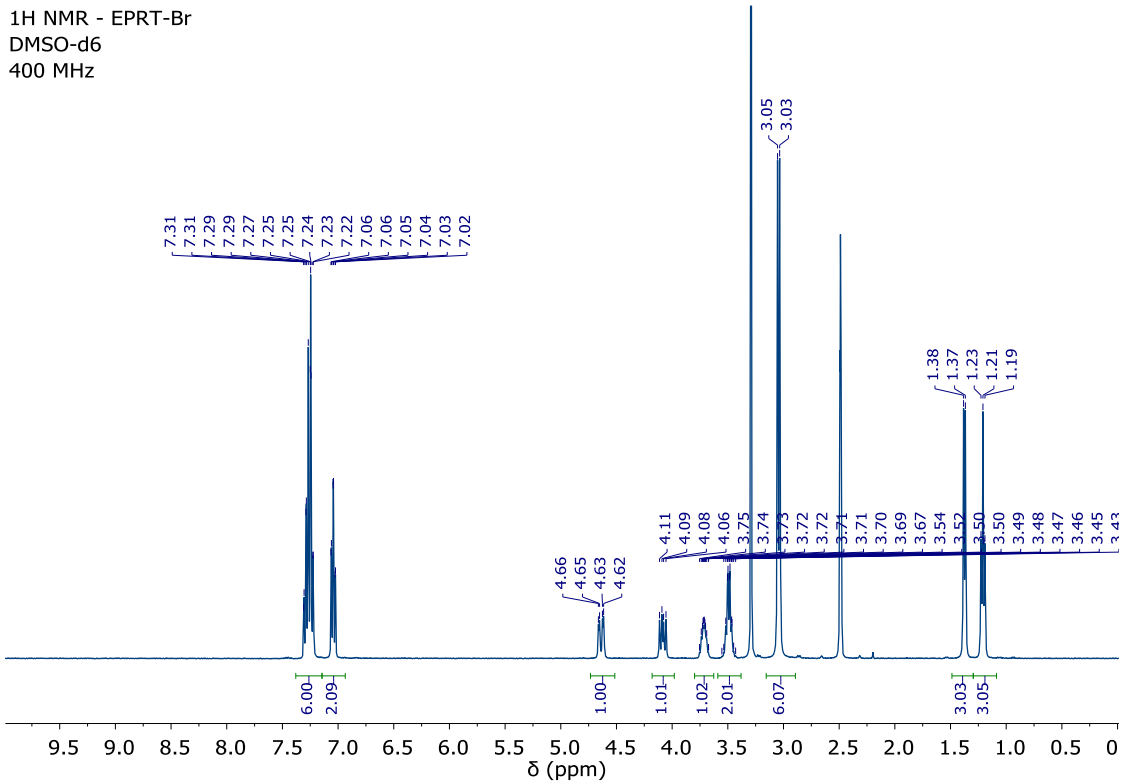

Figure S1. ^{1}H NMR spectrum of EPRT-Br in DMSO-d_6.

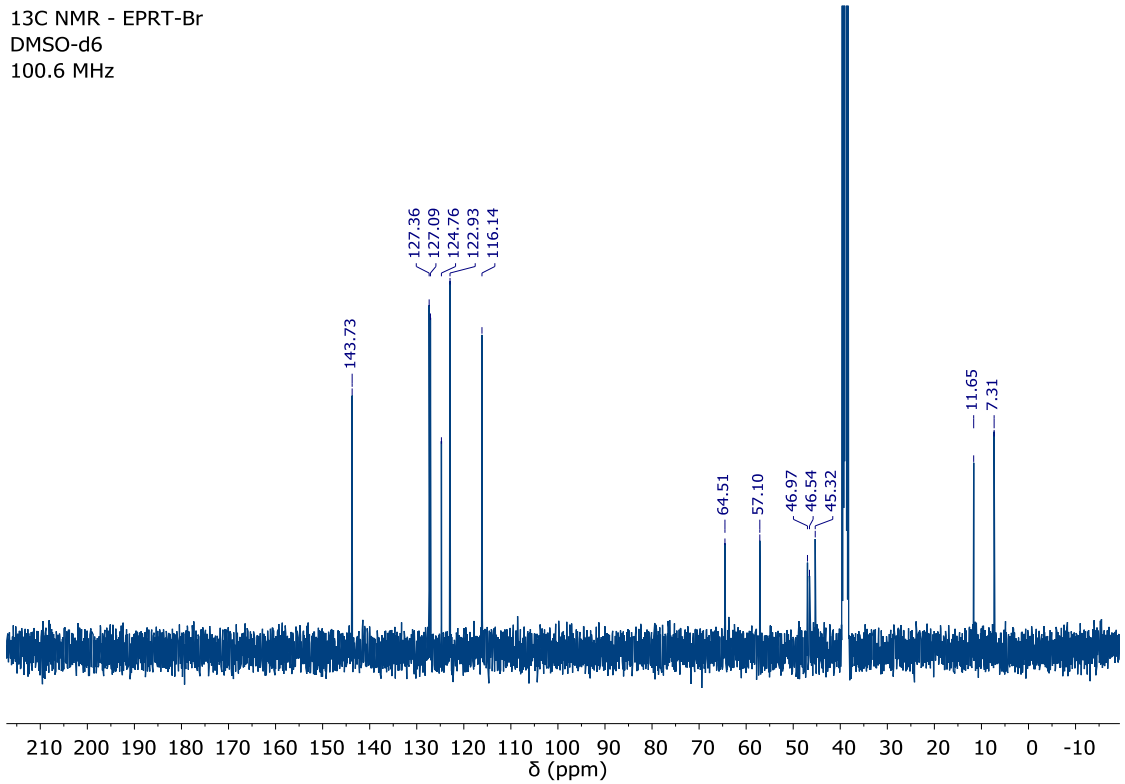

Figure S2. ^{13}C NMR spectrum of EPRT-Br in DMSO-d_6.

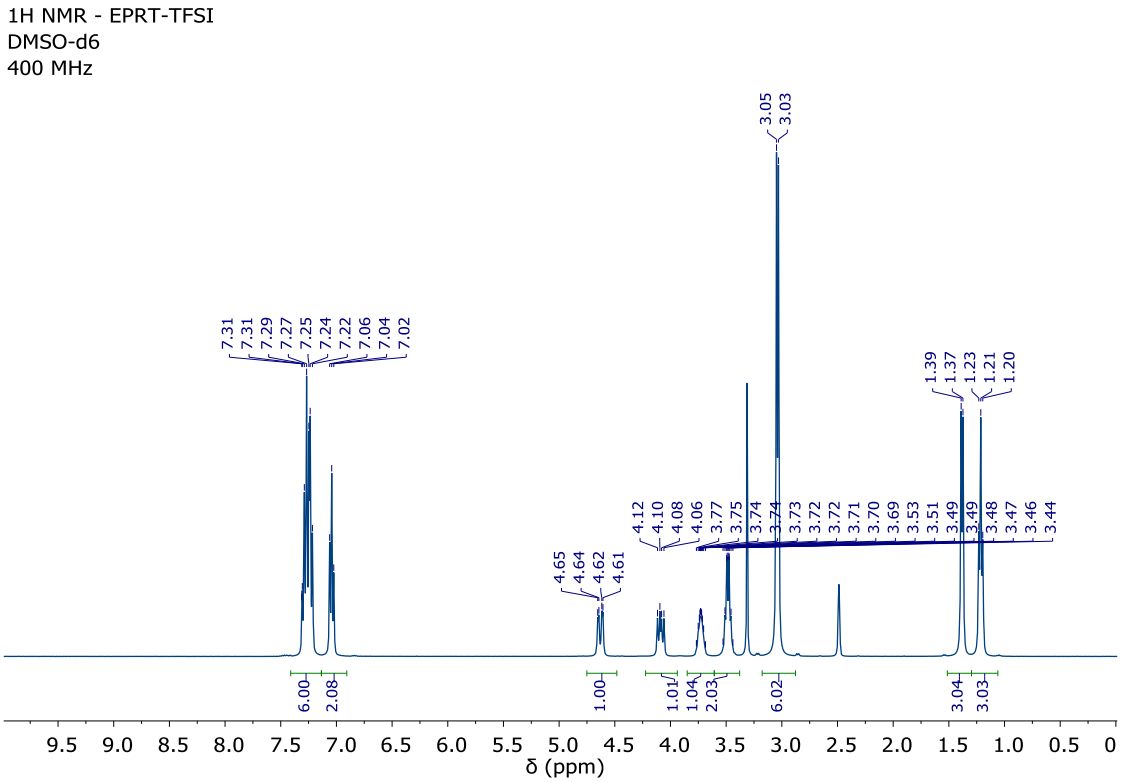

Figure S3. ^{1}H NMR spectrum of EPRT-TFSI in DMSO-d_6

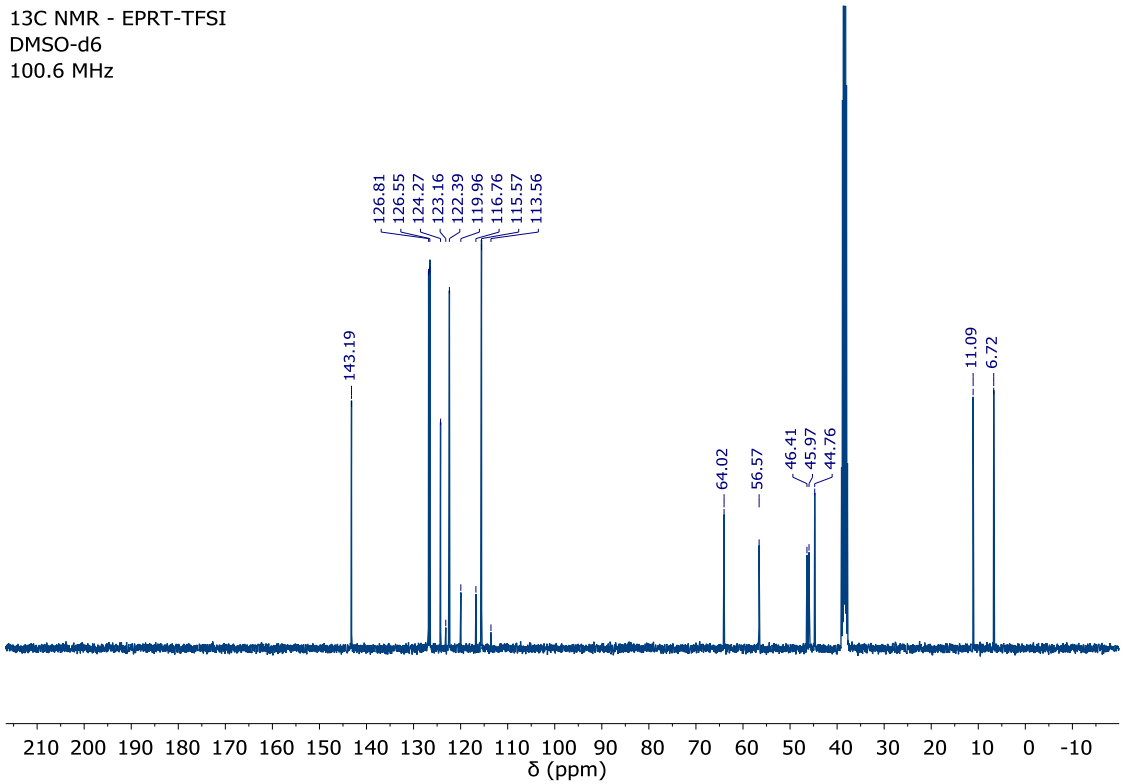

Figure S4. ^{13}C NMR spectrum of EPRT-TFSI in DMSO-d_6.

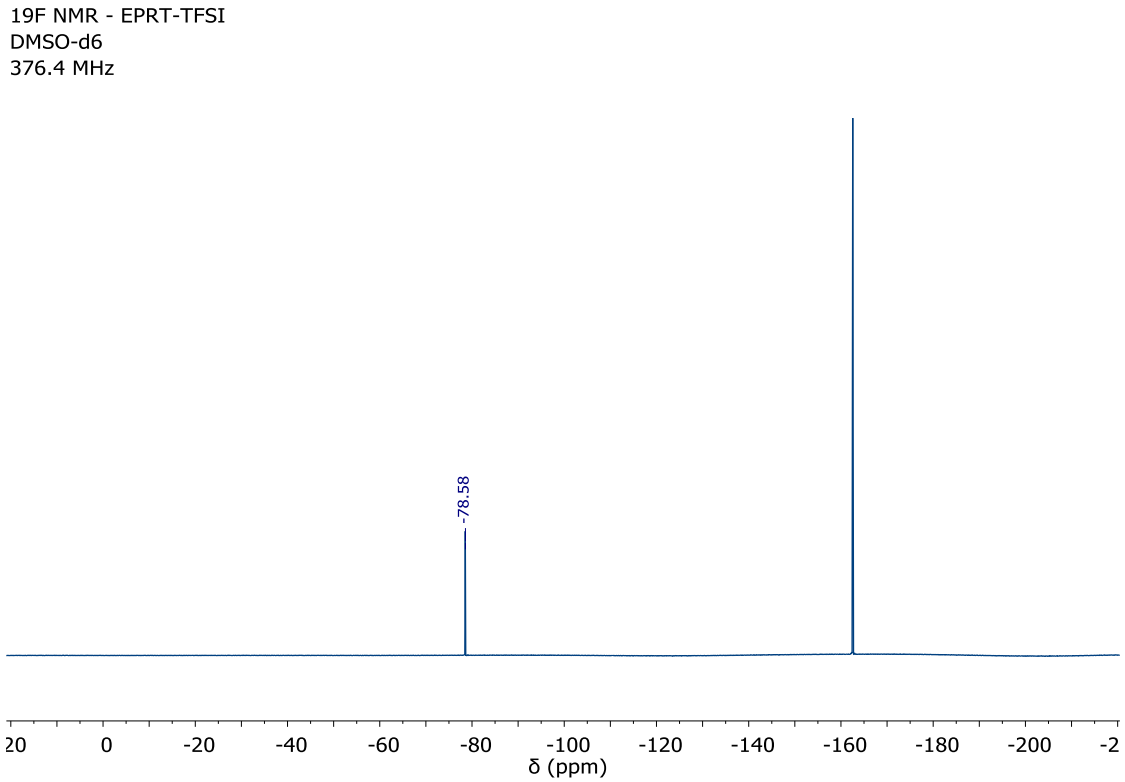

Figure S5. ^{19}F NMR spectrum of EPRT-TFSI in DMSO-d_6.

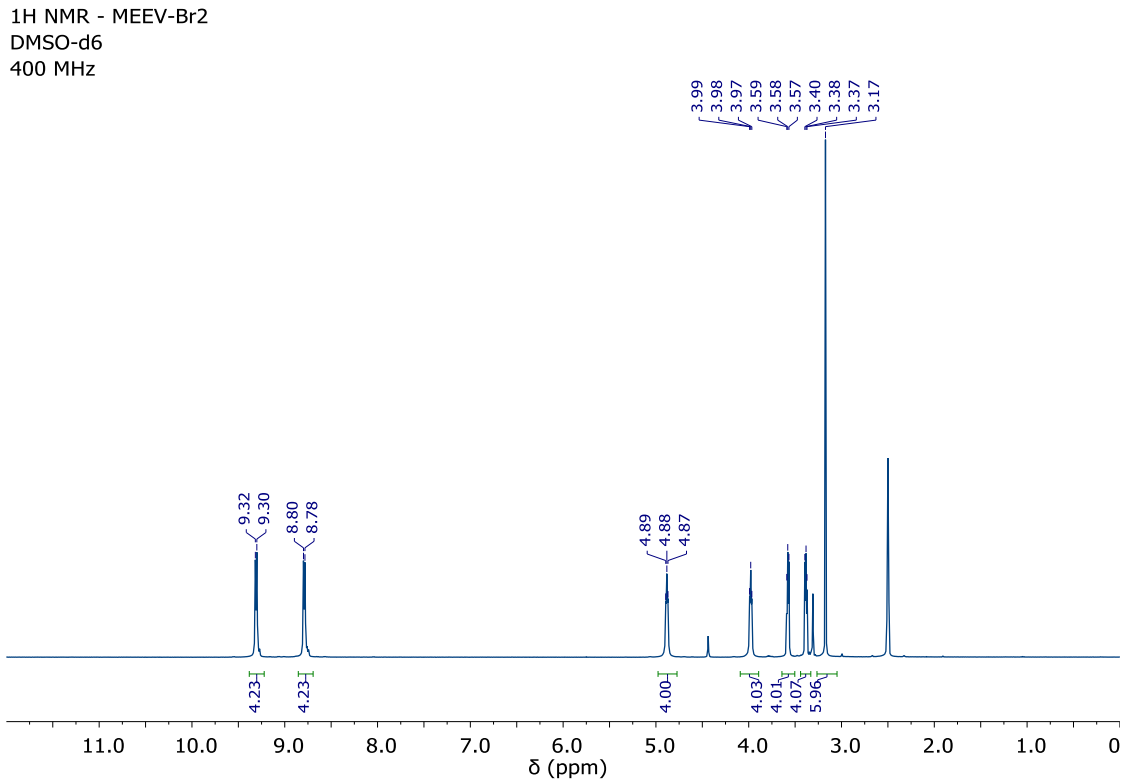

Figure S6. ^{1}H NMR spectrum of MEEV-Br_2 in DMSO-d_6.

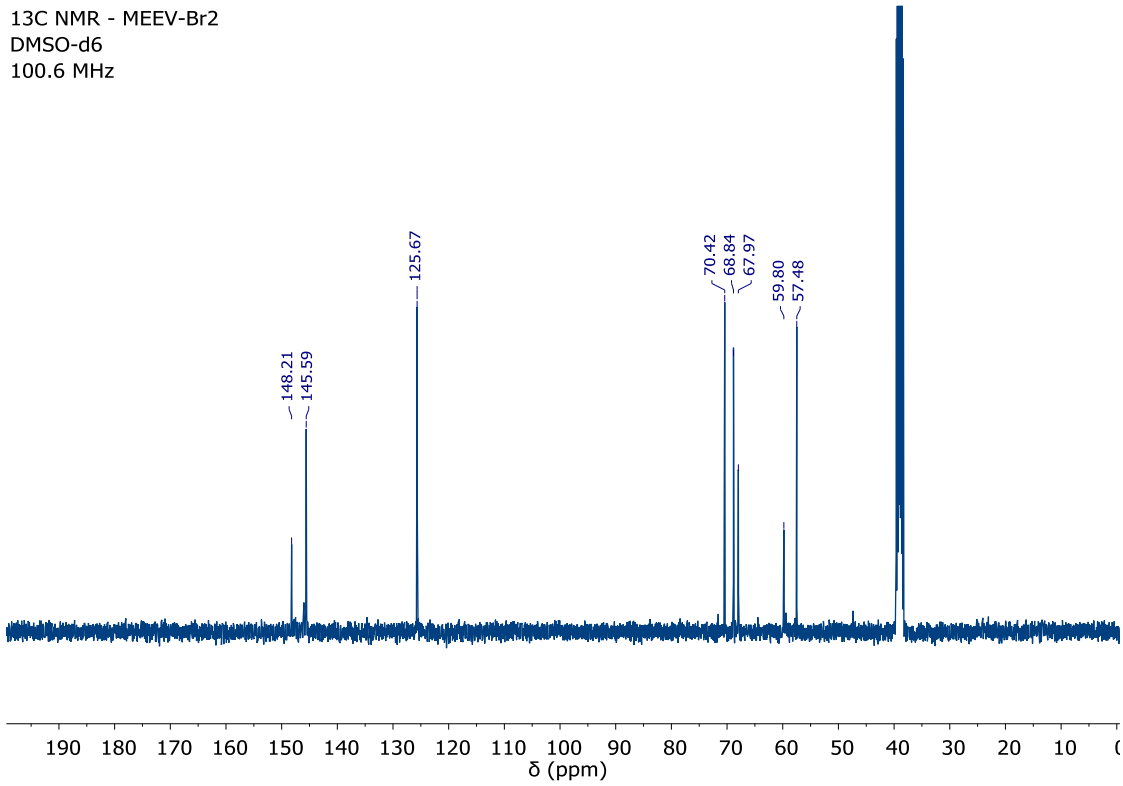

Figure S7. ^{13}C NMR spectrum of MEEV-Br_2 in DMSO-d_6.

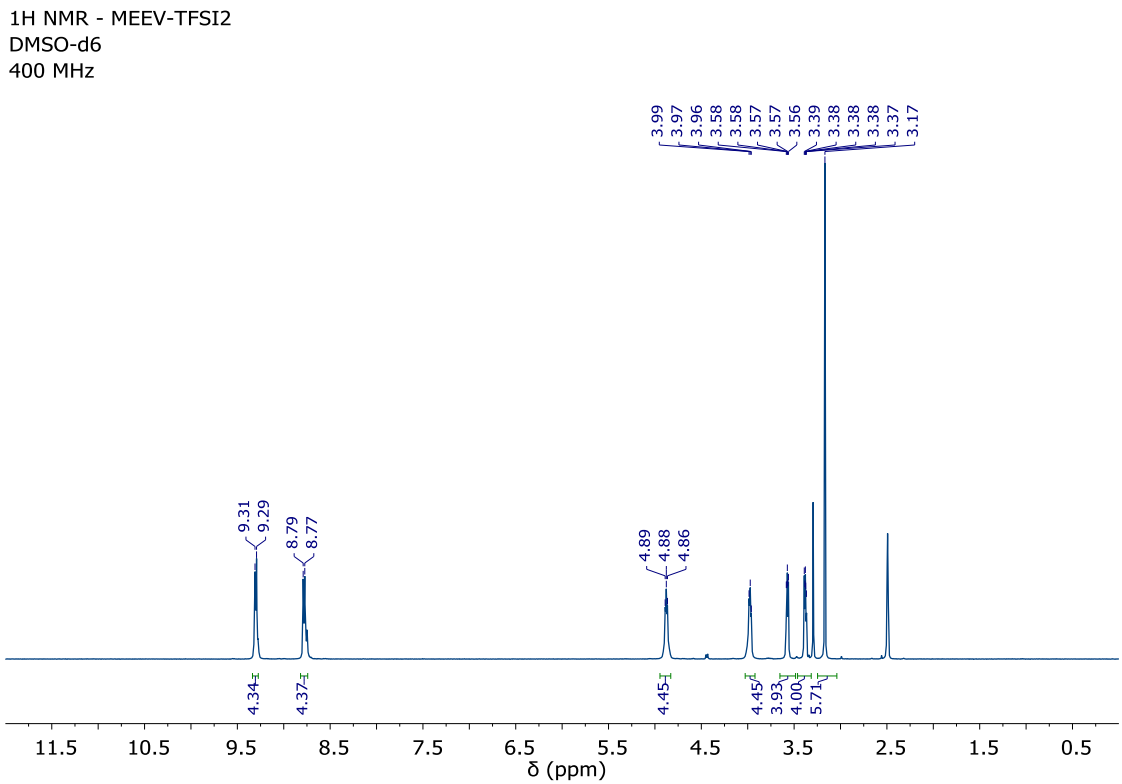

Figure S8. ^{1}H NMR spectrum of MEEV-(TFSI)$_2$ in DMSO-d_6.

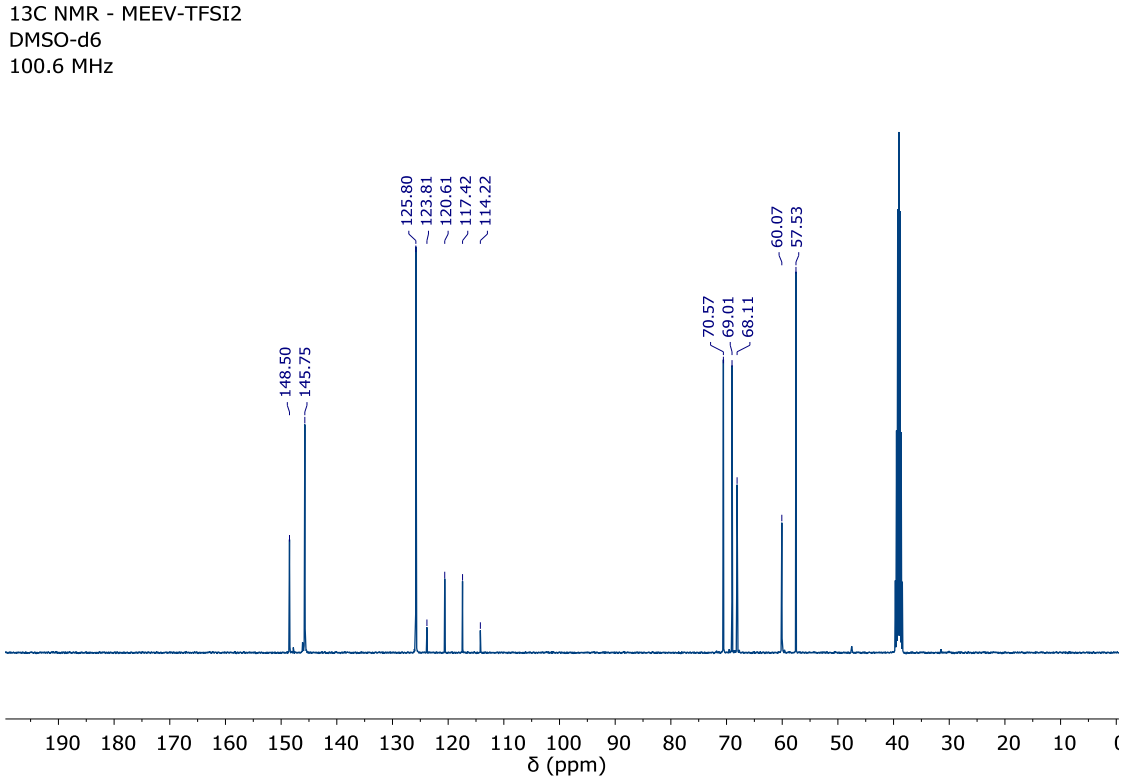

Figure S9. ^{13}C NMR spectrum of MEEV-(TFSI)$_2$ in DMSO-d_6.

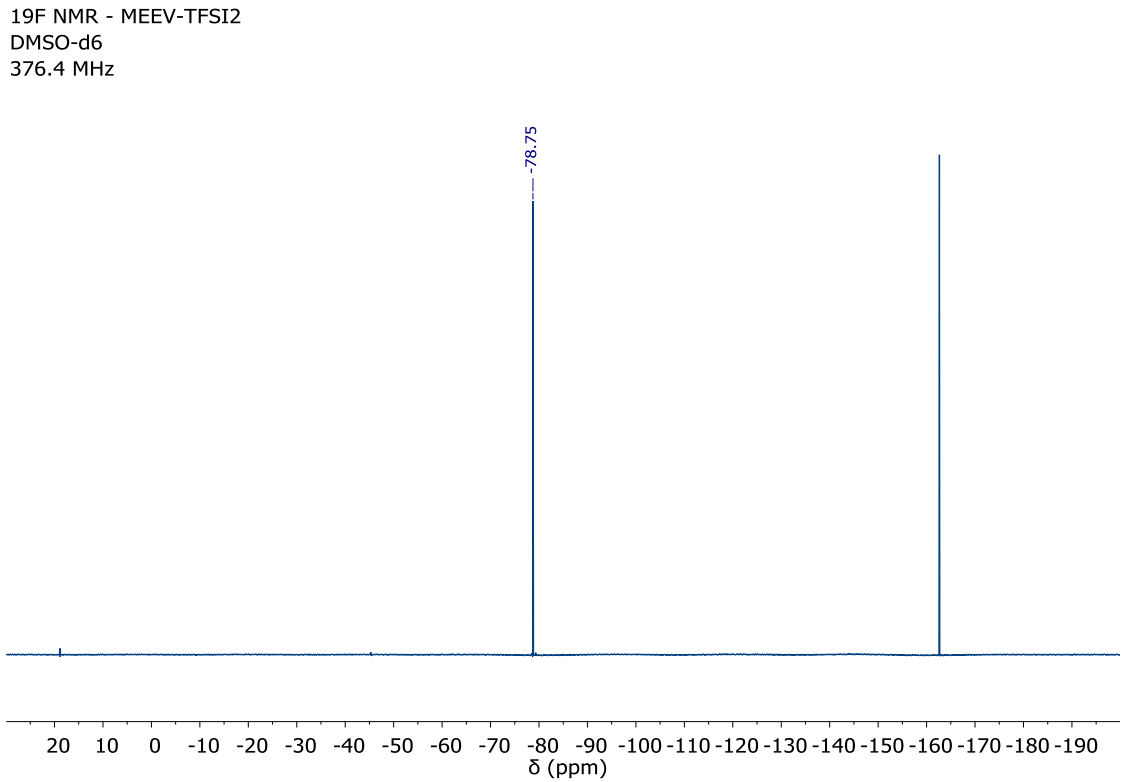

Figure S10. ^{19}F NMR spectrum of MEEV-$(TFSI)_2$ in DMSO-d_6.

IV. X-Ray Crystallography

X-ray diffraction data were collected at 90.0 K on a Bruker D8 Venture kappa-axis diffractometer using MoK(alpha) X-rays. Raw data were integrated, scaled, merged and corrected for Lorentz-polarization effects using the APEX3 package.[2] Corrections for absorption were applied using SADABS.[3] The structure was solved by direct methods (SHELXT)[4] and refinement was carried out against F^2 by weighted full-matrix least-squares (SHELXL).[5] Hydrogen atoms were found in difference maps, but subsequently placed at calculated positions and refined using a riding model. Non-hydrogen atoms were refined with anisotropic displacement parameters. Atomic scattering factors were taken from the International Tables for Crystallography.[6]

V. Ionic Conductivity Viscosity, and Diffusivity

V.1. Ionic Conductivity

Ionic conductivity measurements were carried out on EPRT-TFSI, MEEV-$(TFSI)_2$, and TEATFSI at 0.25, 0.50, 0.75, and 1.00 M in ACN. Measurements were performed with an Orian star A212 conductivity meter (Thermo Scientific) at 25 °C. The conductivity probe was calibrated prior to the measurements using standard solutions (1.413, 12.9, 25, 47.6, 80 mS cm^{-1}, Oakton and

RICCA). For each concentration, 15 mL of sample was used to measure the conductivity, and three measurements were taken; the reported conductivities are the average of the three results. Between each measurement, the probe was washed with anhydrous ethanol and dried to avoid contamination.

V.2. Viscosity

The dynamic viscosity of ionic electrolytes (EPRT-TFSI, MEEV-$(TFSI)_2$, and TEATFSI) were measured in ACN at 0.25, 0.50, 0.75, and 1.00 M. All the measurements were carried out at 25 °C. 2-3 mL of electrolyte solution was used to measure the viscosity at each concentration and measurements were triplicated to calculate the average viscosity. The dynamic viscosity of solutions was measured using a microfluidic pressure-driven flow viscometer (m-VROC, RheoSense, Inc.). The measuring chip contains a rectangular slit flow channel with uniform cross-section area (50 μm × 2 mm). The fluid sample was pushed by a syringe pump at a constant volume flow rate Q and the pressure drop Δpover a length of channel L was measured.

Four pressure sensors are flush-mounted at the boundary wall in the channel and the shear stress at the wall was calculated from the pressure drop as

$$\tau = \frac{\Delta p}{L}\frac{wh}{2w+2h} \quad (1)$$

where Δp is the average measured pressure drop over the length L (15 mm). The known flow rate Q is related to the apparent shear rate at the wall, assuming a Newtonian fluid, by

$$\dot{\gamma}_{app} = \frac{6Q}{wh^2} \quad (2)$$

where $\dot{\gamma}_{app}$ is the apparent shear rate at the wall, w and h are the width and height of the channel respectively. For non-Newtonian fluids (non-constant viscosity), the actual shear rate at the wall $\dot{\gamma}$ is related to apparent shear rate $\dot{\gamma}_{app}$ as

$$\dot{\gamma} = \frac{\dot{\gamma}_{app}}{3}\left[2 + \frac{d\ln\left(\dot{\gamma}_{app}\right)}{d\ln\left(\tau\right)}\right] \quad (3)$$

For Newtonian solutions, which were observed in this study, τ is linearly proportional to $\dot{\gamma}_{app}$, so the shear rate at wall $\dot{\gamma}$ is equal to the apparent shear rate $\dot{\gamma}_{app}$. The dynamic viscosity is defined as:

$$\eta = \frac{\tau}{\dot{\gamma}} \quad (4)$$

Experimental limits were obtained based on the maximum and minimum pressure drop that the sensors can measure and the maximum flow rate of the syringe pump, as shown in the gray lines of viscosity versus shear rate plots. For each solution, viscosity was measured within a wide shear rate range (5 000 – 30 000 s^{-1}). Newtonian behavior was observed (less than 10% variation) for this range of shear rate for all samples. The temperature was controlled at 25 °C by a Thermocube circulator.

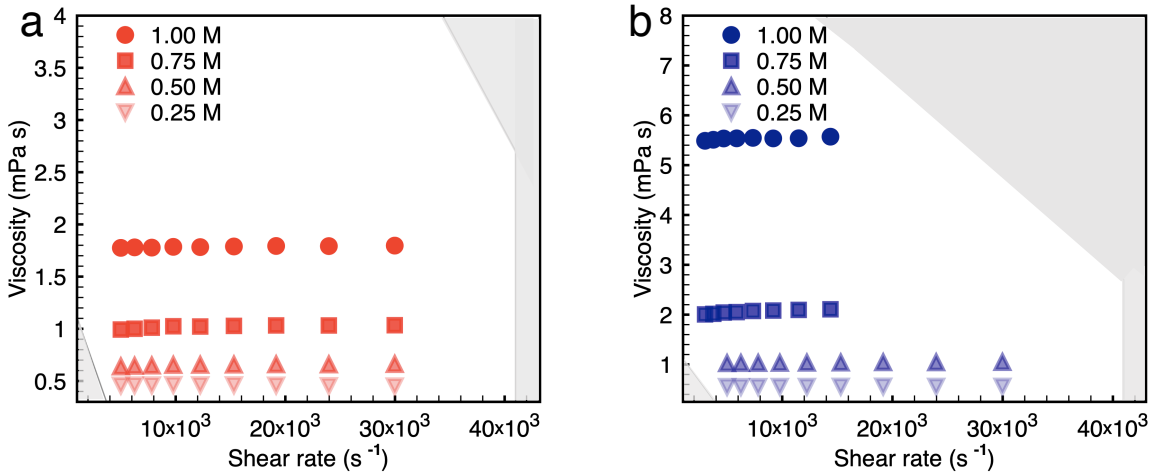

Figure S11. Dynamic viscosity as a function of shear rate at 0.25, 0.50, 0.75, and 1 M for EPRT-TFSI (a), MEEV-$(TFSI)_2$ (b) in acetonitrile. The gray area represents the experimental limits, which comes from the maximum and minimum pressure drops the sensor can measure, and the maximum flow rate.

V.3. Diffusivity (NMR Method)

Diffusion coefficients of cationic species of ionic electrolytes ($EPRT^+$, $MEEV^{2+}$, and TEA^+) were determined by a pulse gradient NMR method at 0.25, 0.50, 0.75, and 1.00 M in CD_3CN. Spectra from samples of varying concentrations were collected on a 500 MHz JEOL ECZr spectrometer (Peabody, MA, USA) equipped with a Royal Probe. In all cases, the gradients were arrayed from 6 mT/m to 280 mT/m linearly over 32 increments. The pw90 was calculated to be 8.12, 7.914, 7.892 µs for EPRT-TFSI MEEV-$(TFSI)_2$, and TEATFSI, respectively. The spectral width was set to 15 ppm with the offset at 5 ppm and the temperature was held at 25 °C. 8 scans, along with 4 pre-scans, were collected for each sample. A JEOL standard pulse sequence 'bpp_led_dosy_pfg' was used to collect the spectra. The peak at 7.01, 8.38, 3.13 ppm was used for curve fitting for EPRT-TFSI, MEEV-$(TFSI)_2$, and TEATFSI, respectively. Diffusion times for each sample were determined via the min and max gradients (6mT/m and 280mT/m) which resulted in ca. 90% reduction in peak height of the ^1H NMR of the sample, using the same parameters as the arrayed

spectra. JEOL Delta 5.0.3 software was used for curve fitting analysis and calculation of the diffusion constant. All experiments were done with JOEL's default gradient settings.

V.4. Comparison of Measured and Estimated Ionic Conductivity

Understanding the ion transport properties is important in designing new redox active molecules and optimizing fluid batteries. A great number of methods have been proposed to find the relation between viscosity, diffusion coefficient, and conductivity of electrolytes,[7-10] from which ion interaction can be determined. Here we use the Nernst-Einstein equation and Stokes-Einstein equation to predict the ionic conductivity of ionic electrolytes from measured viscosity $\eta(c)$ and cationic diffusion coefficient $D_+(c)$ as functions of concentration, then compare with the measured values.

The ionic conductivity of an electrolyte can be estimated from the diffusion coefficients (mobilities) of the charged species by applying the Nernst-Einstein equation,[11]

$$\begin{aligned}\sigma &= \sigma_+ + \sigma_- \\ &= \left(cN_A v_+\right)\left(z_+ e\right)^2 \frac{D_+}{kT} + \left(cN_A v_-\right)\left(z_- e\right)^2 \frac{D_-}{kT} \quad (5) \\ &= \frac{cN_A e^2}{kT}\left(v_+ z_+^{\,2} D_+ + v_- z_-^{\,2} D_-\right)\end{aligned}$$

where σ_+ and σ_- are the conductivities of cation and anion, c is the concentration (mole per volume) of the ion pair, N_A is the Avogadro constant, v_+ and v_- are the numbers of cation and anion per ion pair, z_+ and z_- are the charge numbers of the cation and anion, e is the elementary electric charge, k is the Boltzmann constant, T is the absolute temperature, and D_+ and D_- are the diffusion coefficients of cation and anion. The Nernst-Einstein equation is defined in the dilute regime where there is no ion interaction or ion association, and is based on the Einstein relation that the mobility factor μ relating applied force to velocity is also related to diffusivity as $D = \mu kT$.

The Stokes-Einstein equation further specifies the mobility factor μ based on viscous Stokes flow around a sphere of radius r, so that the diffusivities can be written as

$$D_+ = \frac{kT}{6\pi r_+ \eta} \qquad D_- = \frac{kT}{6\pi r_- \eta} \quad (6)$$

where η is the viscosity of solution, and r_+ and r_- are the hydrodynamic radii of cation and anion, respectively. The Stokes-Einstein equation is also defined in the dilute regime, and it assumes the charge carrier is a Brownian solid sphere, while the Reynolds number of the flow (Re) is much lower than 1.

From viscosity measurement in the dilute limit, we have,[12]

$$\frac{\eta}{\eta_0} = 1 + [\eta]c = 1 + \frac{5}{2} V N_A c \quad (7)$$

where $[\eta]$ is intrinsic viscosity, and V is the total hydrodynamic volume, which is related to the effective hydrodynamic radii by

$$V = \nu_+ \frac{4}{3}\pi r_+^3 + \nu_- \frac{4}{3}\pi r_-^3. \quad (8)$$

To estimate conductivity with equation (5), we need both D_+ and D_-, but D_- was not measured directly. We can estimate it from our viscosity measurements. We use $\eta(c = 0.25\ \text{M})$ to infer r_+ from equation (6), and concentration-dependent viscosity in the linear regime to infer effective hydrodynamic volume V from equation (7), and subsequently estimate r_- from equation (8).

From equation (6), the measured viscosity η and diffusion coefficient D_+ of cations at 0.25 M imply effective hydrodynamic radii of cations r_+ of $EPRT^+$, $MEEV^{2+}$, and TEA^+, which are 5.51, 5.12, and 3.50 Å, respectively. Then the total hydrodynamic volume V of each species was calculated from equation (7) using their measured viscosity at 0.25 M, as shown in Figure S12. Combining the hydrodynamic volumes V and the cation radii r_+, the effective radii r_- of anions ($TFSI^-$) was determined using equation (8), which are 3.84, 5.05 and 4.10 Å, in EPRT-TFSI, MEEV-$(TFSI)_2$, and TEATFSI. The effective radius of $TFSI^-$ in MEEV-$(TFSI)_2$ is larger than the others because it is no longer in the dilute regime compared to the other two ionic electrolytes as evidenced by measured viscosity data at 0.25 M (MEEV-$(TFSI)_2$ has the highest viscosity at 0.25 M). Therefore, the calculated hydrodynamic volume of MEEV-$(TFSI)_2$ is larger than the hydrodynamic volume of the other two ionic electrolytes at 0.25 M which makes the radius of $TFSI^-$ in MEEV-$(TFSI)_2$ larger than its actual value.

Equation (6) shows that for a given viscosity at each concentration, the ratio of diffusivities of cation and anion is inversely proportional to the ratio of hydrodynamic radii, so at each concentration studied, the anion diffusion coefficient $D_-(c)$ can be determined from the measured cation diffusivity and the estimated hydrodynamic radii of cation and anion in each species as $D_-(c) = \frac{r_+}{r_-} D_+(c)$. Finally, the conductivity can be calculated from equation (5).

The calculated and measured conductivities are shown in Figure S13. The results show that the estimated conductivity is slightly larger for EPRT-TFSI and TEATFSI, which is as expected because the prediction is in the ideal case, without ion interaction or ion associations. For MEEV-$(TFSI)_2$ the estimated values are smaller than the measured values, because of the higher hydrodynamic volume, and the higher anionic radius as mentioned before results in a lower anion diffusion coefficient.

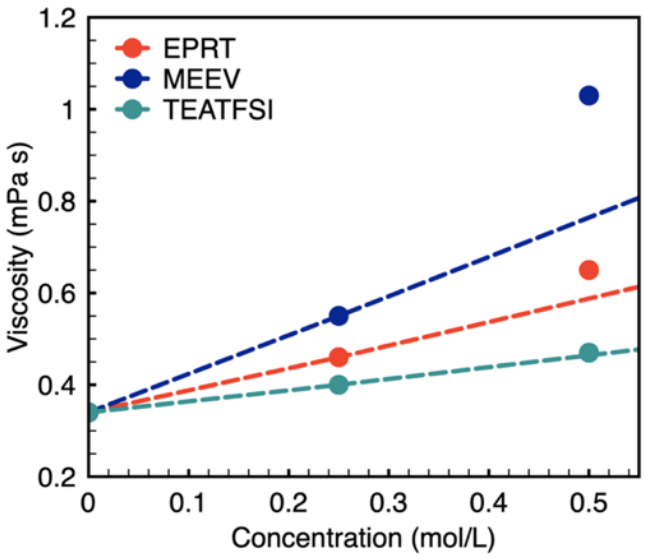

Figure S12. The Newtonian viscosity of EPRT-TFSI, MEEV-$(TFSI)_2$, and TEATFSI as a function of concentration. The slope of the dashed line is proportional to the hydrodynamic volume in the dilute limit (equation (7)); higher order effects (at higher concentrations) are neglected, as the line is fit to data only up to 0.25 M.

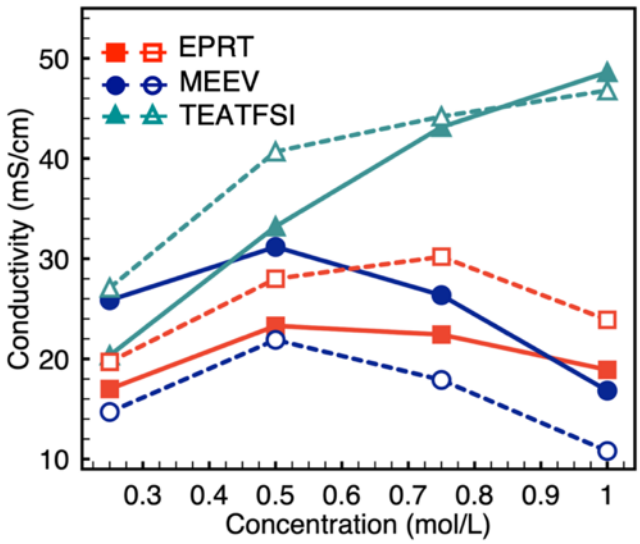

Figure S13. Measured (solid lines) and predicted conductivities (dotted lines) of EPRT-TFSI, MEEV-$(TFSI)_2$, and TEATFSI at 0.25, 0.50, 0.75, and 1.00 M in ACN. Estimates are based on measured viscosity η in the dilute limit (c = 0 – 0.25 M), and measured cation diffusivity $D_+(c)$ at each concentration shown.

Table S1. Ionic conductivity, viscosity, and diffusivity (cationic species) of electrolytes at 0.25, 0.50, 0.75, and 1.00 M of EPRT-TFSI, MEEV-$(TFSI)_2$, and TEATFSI in ACN.

Solution	Concentration (M)	Conductivity (mS cm^{-1})	Viscosity (mPa s)	Diffusivity (x 10^{-6} cm^2 s^{-1})
ACN	N/A	6 x 10^{-10} [(a)]	0.34 [(a)]	N/A
EPRT-TFSI in ACN	0.25	17.00±0.18	0.458±0.04	8.62
	0.50	23.30±0.12	0.652±0.008	6.12
	0.75	22.43±0.12	1.02±0.02	4.40
	1.00	18.91±0.21	1.78±0.01	2.62
MEEV-$(TFSI)_2$ in ACN	0.25	25.86±0.09	0.556±0.003	7.75
	0.50	31.18±0.32	1.03±0.01	5.78
	0.75	26.36±0.06	2.07±0.04	3.16
	1.00	16.83±0.12	5.53±0.03	1.43
TEATFSI in ACN	0.25	20.35±0.15	0.396±0.002	15.6
	0.50	33.22±0.39	0.472±0.001	11.7
	0.75	43.14±0.13	0.560±0.030	8.46
	1.00	48.63±0.42	0.687±0.040	6.73

The diffusivity of cationic, $EPRT^+$, $MEEV^{2+}$, and TEA^+ were measured in CD_3CN.
(a) Ref. (13).

VI. Cyclic Voltammetry

Cyclic voltammetry (CV) measurements were performed in an argon-filled glovebox (MBraun, UNIlab) using 650E potentiostat (CH Instruments, Inc.). CVs were recorded in either ACN or 0.5 M TEATFSI/ACN using a three-electrode system with 3 mm diameter glassy carbon as the working electrode (CH Instruments, Inc.), freshly anodized Ag/AgCl wire as the reference electrode (CH Instruments, Inc.), and a Pt wire as the counter electrode (CH Instruments, Inc.) at active materials concentration of 10 mM. Before each measurement, the working electrode was polished on a MicroCloth pad containing an aqueous slurry of 0.05 μm alumina powder (Buehler Ltd.), rinsed with deionized water, and dried under nitrogen. Ferrocene was used as the internal reference and redox potentials were reported with respect to the ferrocene/ferrocenium ($Cp_2Fe^{0/+}$) redox couple. The half-wave redox potential ($E_{1/2}$), peak height ratio (chemical reversibility), and peak separation (electrochemical reversibility) were calculated for each redox event at a scan rate of 100 mV s^{-1}. 100% iR correction was applied to compensate the solution resistance. The solution resistance was determined using iR compensation technique (CH Instruments 650E potentiostat). The resistance measured was from 700 (for MEEV-$(TFSI)_2$) to 1200 Ω (for EPRT-TFSI) for the active species in ACN and about 60 Ω for the active species in 0.5 M TEATFSI/ACN, which leads to correction of 0.16 (for MEEV-$(TFSI)_2$ in ACN) to 0.21 V (for EPRT-TFSI in ACN) and 0.01 V (active species in 0.5 M TEATFSI/ACN) at the highest current measured. The diffusion coefficients of the active species at 10 mM concentration were calculated using Randles–Sevcik equation,[14]

$$i_p = 0.4463\, nFAc\left(\frac{nFD}{RT}\nu\right)^{0.5} \quad (9)$$

where i_p is the peak current (A), n is the number of electrons transferred (-), F is the Faraday constant (96485 C mol^{-1}), A is the electrode area (cm^2), c is the concentration (mol cm^{-3}), D is the diffusion coefficient (cm^2 s^{-1}), R is the gas constant (8.314 J mol^{-1} K^{-1}), T is the absolute temperature (K), and v is the scan rate (V s^{-1}). The following scan rates were used for diffusion coefficient calculations: 10, 25, 50, 75, 100, 200, 300, 400, and 500 mV s^{-1}.

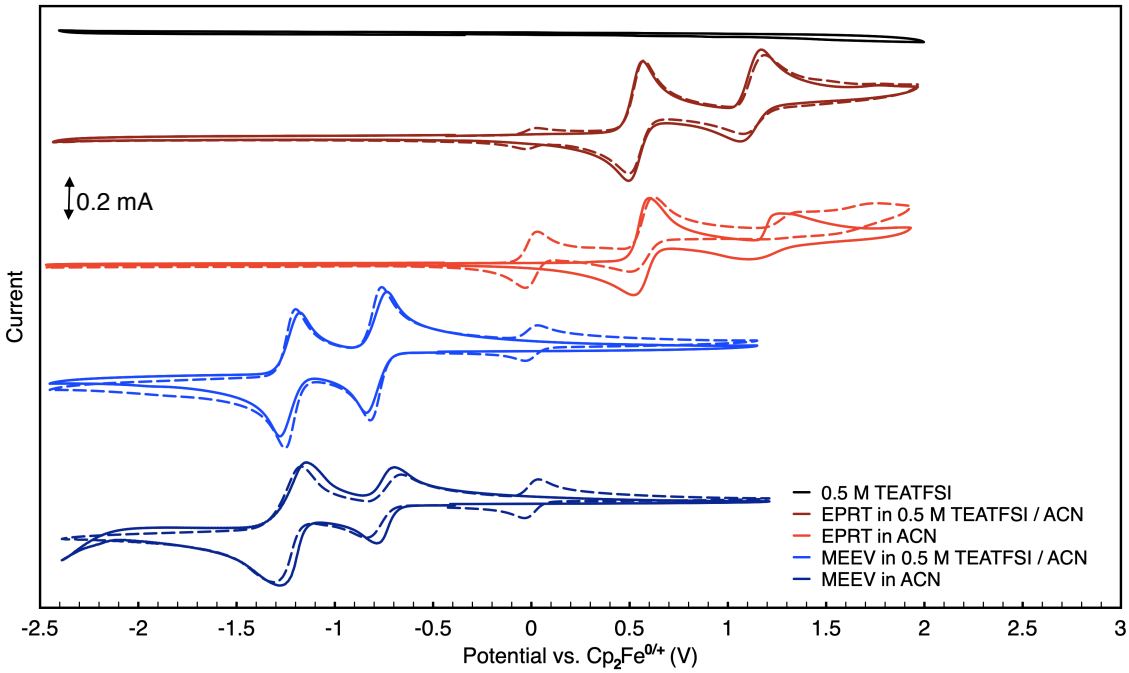

Figure S14. Cyclic voltammograms of EPRT-TFSI and MEEV-$(TFSI)_2$ at 10 mM in ACN, with (dashed lines) or without (solid lines) ferrocene (Cp_2Fe) as an internal reference, recorded at a scan rate of 100 mV s^{-1}. 100% iR correction was applied.

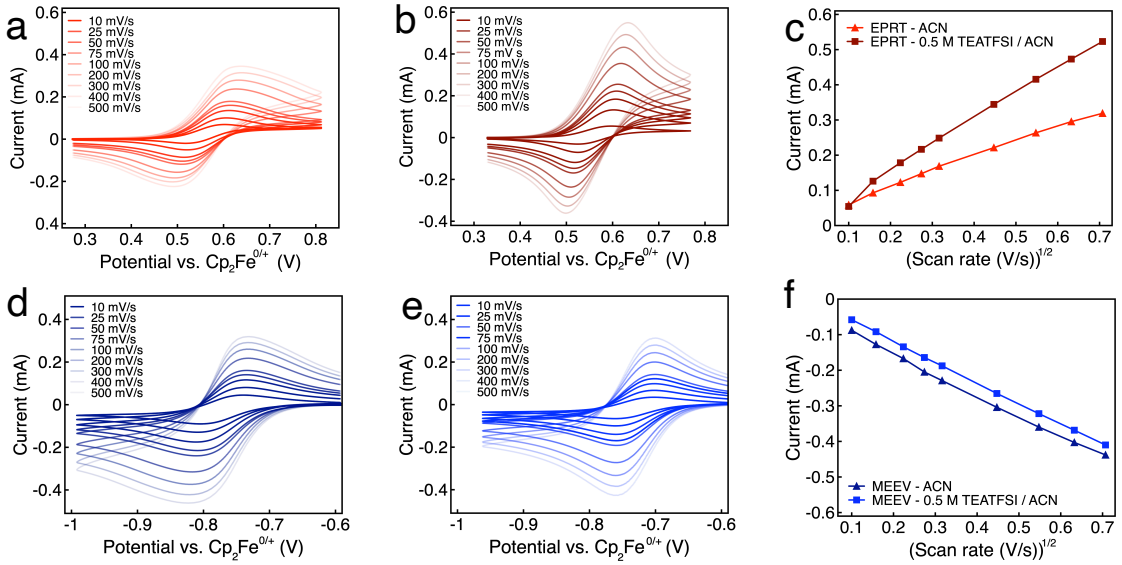

Figure S15. The scan rate-dependent cyclic voltammograms of ionic active species at 10 mM in ACN with no supporting salts and in ACN with 0.5 M TEATFSI. EPRT-TFSI and MEEV-$(TFSI)_2$ in ACN (a,d), and in 0.5 M TEATFSI / ACN (b,e) at scan rates of 10, 25, 50, 75, 100, 200, 300, 400, and 500 mV s^{-1}. Additionally, corresponding Randles–Sevcik plots are shown for EPRT-TFSI (c) and MEEV-$(TFSI)_2$ (f). All cyclic voltammetry experiments were referenced to ferrocene/ferrocenium at 0 V. 100% iR correction was applied.

VII. Solubility

The solubility of EPRT-TFSI and MEEV-$(TFSI)_2$ was determined in ACN and in 0.5 M TEATFSI / ACN. For determination of solubility, a known amount of each material (approximately 0.3-0.5 g) was added to a 3.5 mL glass vial. Then, the electrolyte solution was added slowly (in a period of 30 s), and the solution was sonicated between additions. Electrolyte addition was continued until the active species completely dissolved, as determined by visual inspection. Once completely dissolved, the weight of the solution was recorded. Then, a known volume of aliquot (100 µL) was taken using a micropipette and the weight of the aliquot was recorded to calculate the density of the solution. The total volume of the initial solution was calculated using the density, and then the molarity of the solution was determined as per the calculated volume. This measurement was performed in triplicate for each active species, and the average molar concentrations were calculated.

Table S2. Solubility of EPRT-TFSI and MEEV-$(TFSI)_2$ in ACN and 0.5 M TEATFSI / ACN.

electrolyte	solubility (M)	
	EPRT-TFSI	MEEV-$(TFSI)_2$
ACN	1.27 ± 0.04	1.07 ± 0.02
0.5 M TEATFSI / ACN	1.11 ± 0.01	0.91 ± 0.02

VIII. Crossover

Solutions of 0.2 M active species (MEEPT, EPRT-TFSI, and MEEV-$(TFSI)_2$) were prepared in ACN for crossover analysis via two layers of FAPQ 375 PP. The anion exchange membrane (doubly stacked) FAPQ-375-PP (Fumatech) was pre-soaked in ACN for 24 h prior to the crossover experiment. A solution of active material (3.8 mL) was added to the left side of the H cell and ACN (3.8 mL) was added to the right side. First, CVs of original solutions (0.2 M) were recorded at 5 mM in 0.1 M TEATFSI/ACN by taking 125 µL aliquots and diluting into 4.875 mL of electrolyte solution. Then CVs were recorded at 0, 1, 6, 12, and 24 h by taking 125 µL aliquots from the right side the H cell and following the same dilution into 0.1 M TEATFSI/ACN. Same volume of aliquots (125 µL) were removed from the left side of the H cell to balance the volume at each time. The crossover fractions were calculated by comparing peak currents at each hour to the peak currents of the original CV (0.2 M).

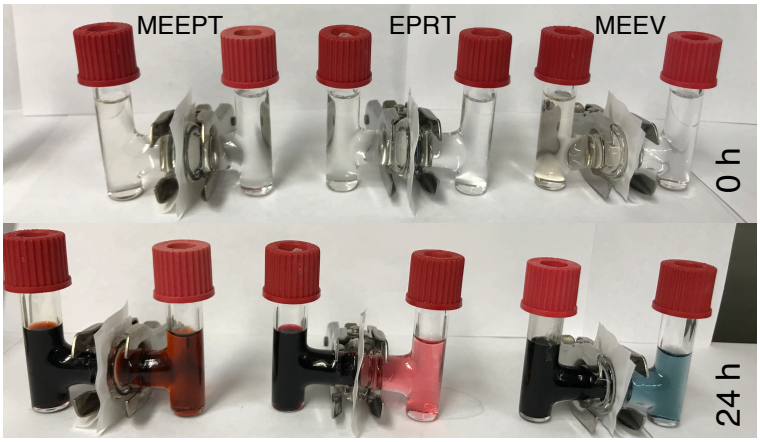

Figure S16. Photographs of H cells for stationary crossover test with two layers of FAPQ-375-PP using MEEPT, EPRT-TFSI, and MEEV-$(TFSI)_2$ (from left to right) as active materials. The left side of the H cell contained 0.2 M active material in ACN, and the right side contained ACN at 0 h. The images were recorded at 0 (top row) and 24 h (bottom row). For 24 h reporting, $NOBF_4$ (for MEEPT and EPRT-TFSI) or Na metal (MEEV-$(TFSI)_2$) was added to the both side of each H cell, which generates colored solutions by either oxidizing (MEEPT and EPRT-TFSI) or reducing (MEEV-$(TFSI)_2$) each active materials.

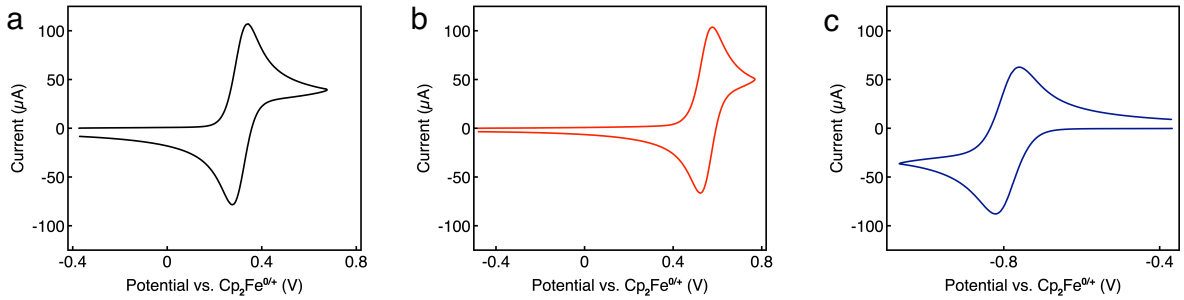

Figure S17. Cyclic voltammograms of 0.2 M original solutions of MEEPT (a), EPRT-TFSI (b) and MEEV-$(TFSI)_2$ (c), recorded at 5 mM in 0.1 M TEATFSI/ACN.

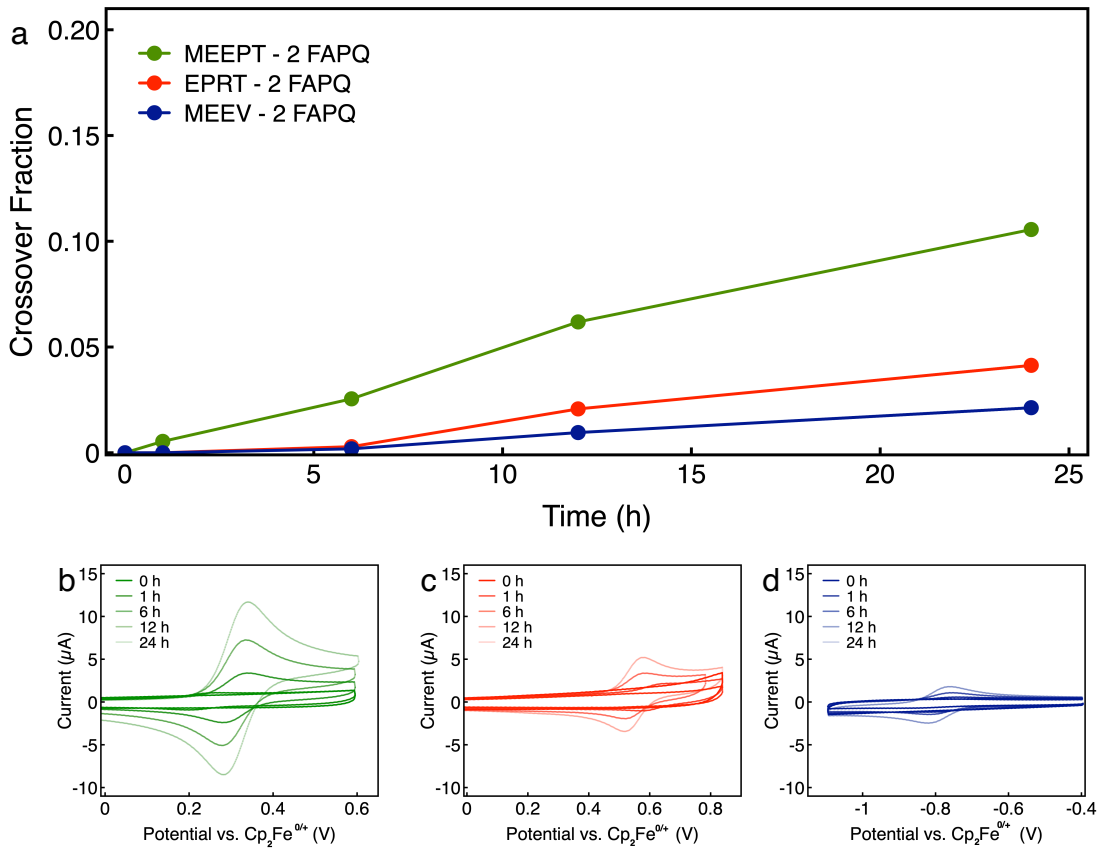

Figure S18. Fraction of crossover vs. time of MEEPT, EPRT-TFSI, and MEEV-$(TFSI)_2$, through two stacks of FAPQ-375-PP (a). Cyclic voltammograms of diluted aliquots taken from the right side of each H cell at 0, 1, 6, 12, and 24 h for MEEPT (b), EPRT-TFSI (c), and MEEV-$(TFSI)_2$ (d) in 0.1 M TEATFSI/ACN.

IX. Impedance Measurements

Impedance measurements were collected in an argon-filled glovebox (MBraun) using VSP potentiostat (BioLogic) using the same custom-built-small volume flow cell (more details in section X) that was utilized for the flow cell experiments. The anion exchange membrane (doubly

stacked) FAPQ-375-PP (Fumatech) was used as received. The electrolyte used in the impedance study contained either 0.5 M TEATFSI (both positive side and negative side) or 0.5 M EPRT-TFSI (positive side) with 0.5 M MEEV-$(TFSI)_2$ (negative side). Impedance spectra were obtained a frequency range of 200 kHz to 10 mHz with 5 points per decade. Impedances were measured under potentiostatic control of the cell and the amplitude of the sinusoidal current was 10 mA. The electrolyte was pumped for 24 h to soak the membrane after which the impedance measurements were recorded.

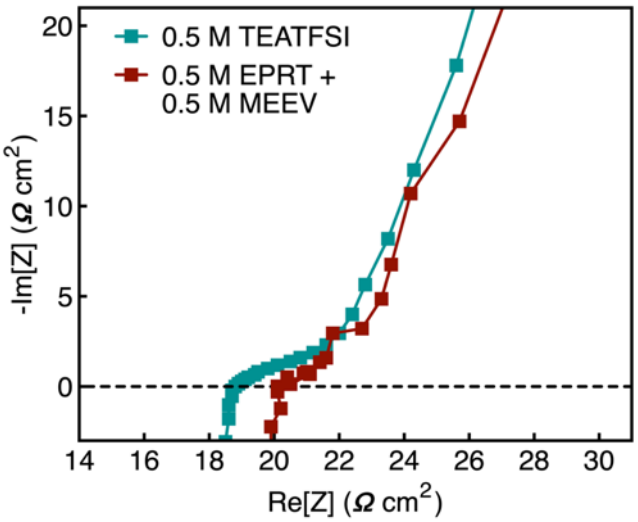

Figure S19. Nyquist plot of the flow cell with two stacked pieces of FAPQ-375-PP anion exchange membrane in electrolyte of 0.5 M EPRT-TFSI / ACN (positive side) and MEEV-$(TFSI)_2$ / ACN (negative side) and 0.5 M TEATFSI / ACN (both sides).

X. Flow Cell Cycling

Small volume custom flow cells with interdigitated flow fields were used during redox flow cell cycling.[15] The backing plates were made from polypropylene, which has chemical compatibility with the materials used in this manuscript. 3.18 mm thick impregnated graphite was used to make the graphite flow fields (product G347B, MWI Inc., Rochester, NY). The size of carbon paper is 1.7 cm × 1.5 cm with 190 ± 30 µm thickness (SGL 29 AA, SGL group, Wiesbaden, Germany) and used as received. Two pieces of carbon paper was layered on each side of the flow cell. FAPQ-375-PP (Fuma-Tech) was used as membrane. The cells were sealed using custom gaskets cut from polytetrafluoroethylene gasket tape (Goretex) with a 2.55 cm^2 geometric area. All flow cells were assembled in the air and then kept in vacuum state for ~ 1 h before transferred into an argon-filled glovebox (MBraun, O_2 < 5 ppm, H_2O < 0.1 ppm).

10 mL perfluoroalkoxy alkane (PFA) jars (Savillex) were used as electrolyte reservoirs and a peristaltic pump (Masterflex L/S Series) was used to carry the electrolyte at a flow rate of 10 mL min^{-1}. Norprene tubing (Masterflex) was used inside the pump head. PFA tubing

(Swagelok) connected the reservoirs to the flow cell. Stainless steel compression fittings (Swagelok) were used to connect the Norprene and PFA tubing. All tubing inner diameters were 1.6 mm.

Two different types of concentrated cells were assembled: 1) 0.5 M EPRT-TFSI / 0.5 M MEEV-$(TFSI)_2$ / separated / ACN / 2FAPQ-375-PP; 2) 0.25 M EPRT-TFSI / 0.25 M MEEV-$(TFSI)_2$ / mixed / ACN / 2FAPQ-375-PP. 10 mL of electrolyte solution was utilized in each side of flow cell. The membranes were soaked in ACN for 24 h before loading samples. Rate and constant current stability studies were performed for each type of flow cell experiments. Data was collected using a VSP potentiostat (BioLogic).

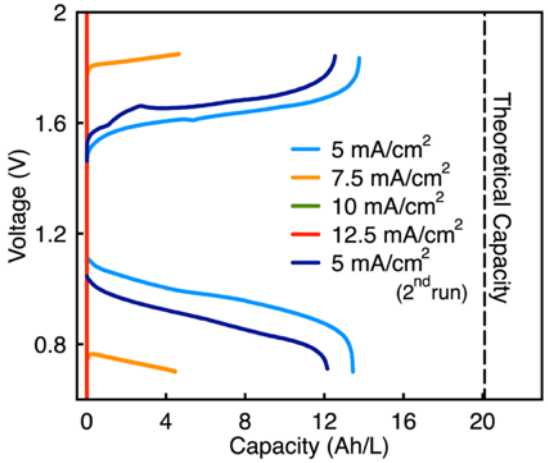

Figure S20. Rate study of EPRT-TFSI and MEEV-$(TFSI)_2$ in a mixed flow cell, showing voltage vs. capacity for various current densities. Potential curves are from the 2nd cycle at each current density. Potential cut-off for flow cell experiment was 1.85 to 0.70 V. Both sides of cell contained 0.75 M EPRT-TFSI and 0.75 M MEEV-$(TFSI)_2$ in ACN with no supporting salt. 10 mL of electrolyte solution was utilized in each side of flow cell.

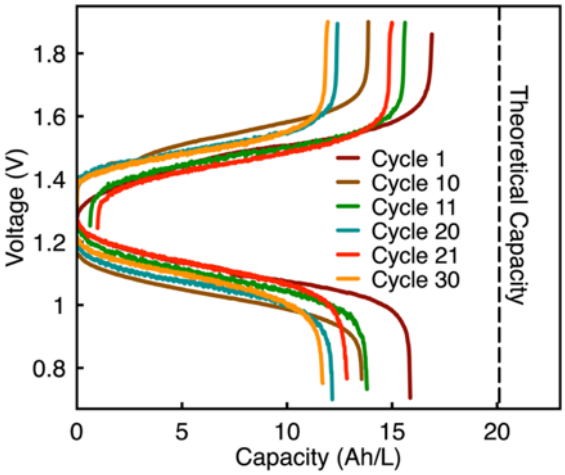

Figure S21. Constant current cycling of EPRT-TFSI and MEEV-$(TFSI)_2$ in a premixed flow cell, showing voltage vs. capacity at 5 mA cm^{-2} current density. Potential cut-off for flow cell experiment was 1.85 to 0.70 V. Both sides of cell contained 0.75 M EPRT-TFSI and 0.75 M MEEV-$(TFSI)_2$ in ACN with no supporting salt. Constant current cycling was stopped at cycle number 10 and 20, then rebalanced and restarted. 10 mL of electrolyte solution was utilized in each side of flow cell.

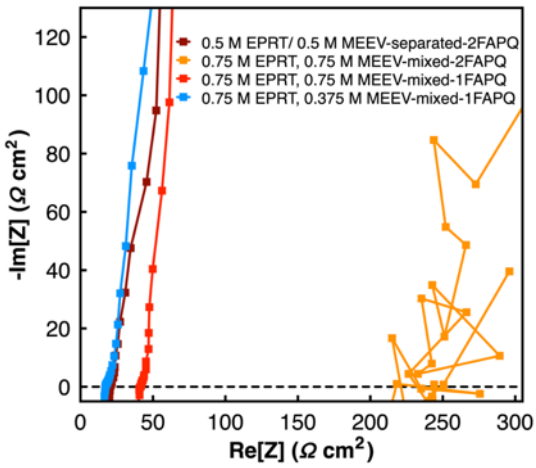

Figure S22. Nyquist plot of the flow cell with one or two stacked pieces of FAPQ-375-PP anion exchange membrane in electrolyte of 0.5 M EPRT-TFSI / ACN (positive side) and MEEV-$(TFSI)_2$ / ACN (negative side), 0.75 M EPRT-TFSI, 0.75 M MEEV-$(TFSI)_2$ / ACN (both sides), and 0.75 M EPRT-TFSI, 0.375 M MEEV-$(TFSI)_2$ / ACN (both sides).

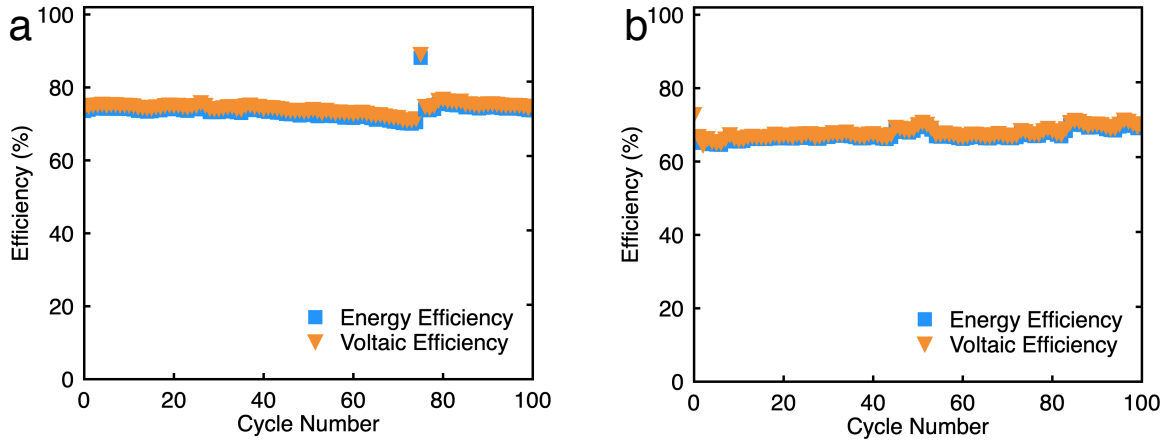

Figure S23. Voltage efficiency and energy efficiency of EPRT-TFSI and MEEV-$(TFSI)_2$ in separated and mixed flow cells in acetonitrile with no supporting salts. Efficiency vs. cycle number for 0.50 M active species in separated flow cell (a) and 0.25 M active species in a mixed flow cell (b).

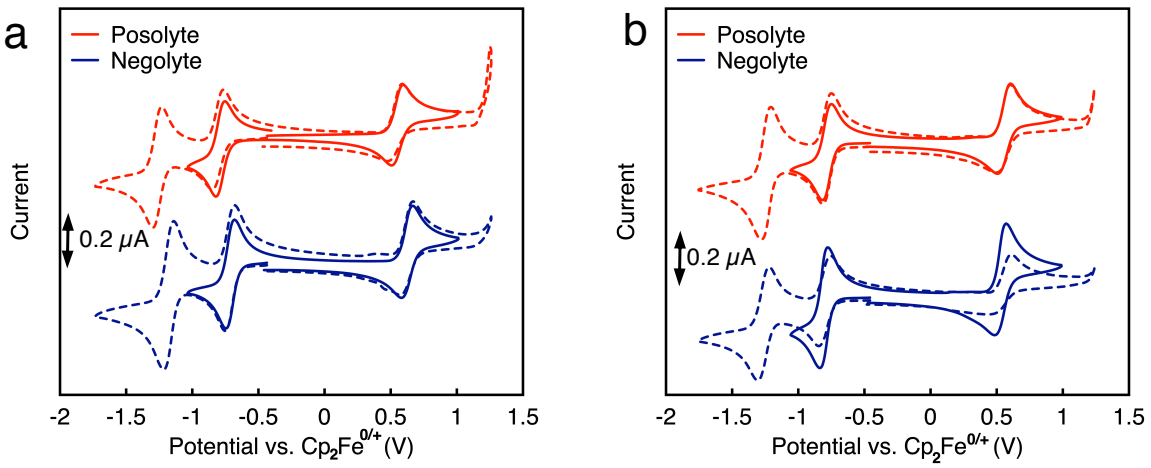

Figure S24. Cyclic voltammetry scans (100 mV s^{-1}) of the posolyte (red) and negolyte (blue) after constant current cycling of separated flow cell (0.5 M EPRT and 0.5 M MEEV-$(TFSI)_2$, after 74 cycles) (a), mixed flow cell (0.25 M EPRT and MEEV-$(TFSI)_2$ in both sides, after 100 cycles) (b) at approximately 10 mM in active material in ACN, solid lines represent the first redox events while dashed lines represent the full window. 100% iR correction was applied.

References

1 A. B. Bate, J. H. Kalin, E. M. Fooksman, E. L. Amorose, C. M. Price, H. M. Williams, M. J. Rodig, M. O. Mitchell, S. H. Cho and Y. Wang, *Bioorg. Med. Chem. Lett.*, 2007, **17**, 1346-1348.

2 Bruker-AXS (2016). APEX3 Bruker-AXS Inc., Madison, WI, USA.

3 L. Krause, R. Herbst-Irmer, G. M. Sheldrick and D. Stalke, *J. Appl. Crystallogr.*, 2015, **48**, 3-10.

4 G. M. Sheldrick, *Acta Crystallogr. A*, 2015, **71**, 3-8.

5 G. M. Sheldrick, *Acta Crystallogr. C*, 2015, **71**, 3-8.

6 Z. Otwinowski and W. Minor, in *Methods Enzymol.*, Elsevier, 1997, vol. 276, pp. 307-326.

7 A. F. Lanord, and J. C. Grossman, *Phys. Rev. Lett.* 2019, **122**, 136001-136007.

8 J. P. Southall, H. V. St. A. Hubbard, S.F. Johnston, V. Rogers, G. R. Davies, J. E. McIntyre, and I. M. Ward, *Solid State Ion*. 1996, **85,** 51-60.

9 K. R. Harris, *J. Phys. Chem.* 2010, **114**, 9562-9577.

10 A. Grandjean, M. Malki, C. Simonnet, D. Manara, and B. Penelon. *Phys. Rev. B* 2007, **75**, 054112.

11 A. Z. Borucka, J. O. M. Bockris, and J. A. Kitchener, *Chem. Phys.* 1956, **24**, 1282-1283.

12 M. L. Huggins, *J. Am. Chem. Soc.* 1942, **64**, 2716–2718.

13 K. Gong, Q. Fang, S. Gu, S. F. Y. Li and Y. Yan, *Energy Environ. Sci.*, 2015, **8**, 3515-3530.

14 R. G. Compton and C. E. Banks, *Understanding Voltammetry*, Imperial College Press, London, 2nd edn., 2011.

15 J. D. Milshtein, J. L. Barton, R. M. Darling and F. R. Brushett, *J. Power Sources*, 2016, **327**, 151-159.